Control of *cis*-Stilbene Photochemistry Using Shaped Ultraviolet Pulses

M. Greenfield,* S. D. McGrane, and D. S. Moore

Dynamic and Energetic Materials Division, Los Alamos National Laboratory, Los Alamos, New Mexico 87545

Received: February 28, 2008; Revised Manuscript Received: November 3, 2008

We demonstrate product branching control of the photoisomerization and cyclization reactions of *cis*-stilbene dissolved in *n*-hexane. An acousto-optical modulator-based pulse shaper was used at 266 nm, in a shaped pump−supercontinuum probe technique, to enhance and suppress the relative yields of the *cis*- to *trans*-stilbene isomerization as well as the *cis*-stilbene to 4*a*,4*b*-dihydrophenanthrene cyclization. Global, local, and single variable optimization control schemes were all successful at controlling stilbene's excited-state intramolecular rearrangements. The presence of multiphoton transitions was determined to be crucial in changing the yield under the experimental conditions employed. We have mapped experimental conditions in which multiphoton absorption was successful in controlling photoproduct branching ratios in stilbene, illustrated that the intensity dependence of the product yields can provide details of reactive channel branching ratios of higher excited-states, and shown that under the experimental conditions employed (150 fs laser) intensity control was the *only* mechanism available to the optimal control methods employed that could affect reaction yields.

Introduction

Since its conceptual advent in the 1980s,[1−3] the field of coherent control has significantly advanced both theoretically[4−16] and experimentally,[17−42] as has been recently reviewed.[17−20] The act of controlling atomic and molecular systems by coherent manipulation of light−matter interactions has been successful in both gas- and condensed-phase systems. The success in condensed phases illustrates that control is possible even with the increased coupling to the environment (solvent molecules), which enhances the intermolecular interactions and decreases the time scale in which the molecular system remains coherent.

Attaining coherent control is performed by adjusting the spectral phase and amplitude of an ultrashort laser pulse,[43,44] in efforts to guide the system dynamics toward a desired product. Due to the commercial availability of visible to near-infrared pulse shapers and the Ti:sapphire fundamental wavelength of 800 nm, a majority of coherent control experiments have been performed using shaped 800 nm pulses.[43−47] However, many molecular systems have strong electronic absorption bands only in the ultraviolet (UV). Consequently, the recent introduction of shaped UV pulses[48−51] lends themselves to a larger range of experiments in which molecular dynamics can be controlled through resonant single-photon excitation.

In this article, we are concerned with the application of optimal coherent control with ultraviolet shaped pulses to the isomerization and cyclization of *cis*-stilbene in an *n*-hexane solution. The reaction dynamics of stilbene have been studied for more than 60 years[52−57] and are relatively well understood. Therefore, the intramolecular rearrangements (isomerization and cyclization) of stilbene's excited-state are ideal for studying under optimal control.

Absorption of a photon at 266 nm resonantly excites *cis*-stilbene to the first excited-state.[58] Once in the excited-state, ∼70% of *cis*-stilbene will move along the isomerization reaction coordinate, while the remaining fraction moves along the cyclization coordinate to form 4*a*,4*b*-dihydrophenanthrene (DHP).[54] Isomerization of *cis*-stilbene occurs on a time scale of ∼1 ps[54−56,59,60] and arises through a conical intersection present between the ground and first excited-state. The conical intersection develops in a region of the excited-state potential energy surface that is twisted ∼90° about the ethylenic bond.[61] Population branches from this twisted region to the cis and trans isomers in roughly a 1:1 ratio, meaning that approximately 33% of the initially excited *cis*-stilbene will isomerize to *trans*-stilbene as it falls back to the ground-state via the conical intersection.[62] The cyclization coordinate also contains a conical intersection[63] through which ∼19%[62] of the initially excited *cis*-stilbene will cyclize to DHP in less than 2 ps.[54]

Herein, we detail experiments that employ phase-shaped 266 nm femtosecond pulses that maximize or minimize the isomerization and/or cyclization of *cis*-stilbene in *n*-hexane. Global and local optimization routines (genetic algorithm, differential evolution, and downhill simplex) as well as single parameter control schemes (linear chirp or pulse energy) are utilized to find optimal pulse shapes and understand the mechanism of their action.

Experimental Section

The laser employed in this work was a Ti:sapphire femtosecond system consisting of a Spectra Physics Tsunami oscillator and Spitfire amplifier. The 1 kHz output had a pulse energy of 1.0 mJ with a center wavelength of 797 nm. The spectral bandwidth was 13 nm full width at half maximum (FWHM) giving pulses of 100−110 fs (FWHM) pulse length.

Multiple Wavelength Generation. The 800 nm pulse was split into two beams, pump and probe, using a 98% beamsplitter. Before entering the pulse shaper, the 0.98 mJ pump beam was frequency doubled using a 250 μm thick β barium borate (BBO) second-harmonic generation crystal. The 0.35 mJ, 400-nm pulse was further mixed with the remaining 800 nm light in a 250 μm BBO third-harmonic generation crystal, creating a 0.1 mJ, 150 fs, 266 nm pulse.

* To whom correspondence should be addressed. E-mail: margog@lanl.gov.

10.1021/jp801758v CCC: $40.75
Published on Web 02/24/2009

Ultraviolet Pulse Shaping. The 266 nm pulse was sent into an acoustic optical modulator (AOM) pulse shaper that consisted of a 4-f zero dispersion compressor.[44,48,50] The pulse was dispersed by a 3600 g/mm grating, and a 0.5-m focal length (fl) spherical mirror was used to focus the beam. A fused silica AOM crystal (Brimrose FSD8-200-100-.400) was positioned in the Fourier plane where an acoustic pulse modulated the index of refraction of the crystal, creating a transmission grating. The relative phase and amplitude of the radio frequency (RF) pulse, used to produce the acoustic pulse, was transferred onto the diffracted light. The shaped RF was generated by mixing a shaped 50−150 MHz RF pulse from a 1 GSample/s arbitrary waveform generator (Gage CompuGen11G) with a 300 MHz oscillator and filtering out the lower frequency 150−250 MHz sideband before amplification to 2 W (MiniCircuits RF components ZFM-4-S, ZX-95-400-S, SHP-150+, SLP-250+, and ZFL-5W-1). The spatial extent of the dispersed spectrum in the Fourier plane and 100 MHz bandwidth of the AOM allowed 150 independent phase (and 150 amplitude) parameters across the entire spectrum. The energy throughput was limited by the gratings, mirrors, and AOM diffraction efficiency to ∼5%.

Transient Absorption and Fitness Measurement. A white light supercontinuum (310−750 nm) was generated by focusing a spatially selected (through an iris) and attenuated fraction of the 800 nm probe pulse into a 2-mm-thick CaF_2 window. Short pass filters were utilized to remove the intense residual 800 nm light. The CaF_2 window was constantly translated along two orthogonal directions to prevent damage and increase the white light stability. The shortest wavelength components were strongly chirped, leading to ∼3 ps of chirp across the spectral range 320−720 nm, as measured by the optical Kerr effect.[64,65] This chirp was removed in the transient absorption data reported via numerical analysis. The timing overlap between the pump and probe at every spectral position was defined as the first point exceeding a threshold above the noise of the differentiated pump−probe signal. As a function of frequency, these time delays were fit to a polynomial and the time axis of each frequency component was shifted to remove the effect of white light chirp on the pump−probe spectra. The accuracy of this shift was approximately equal to the pulse width, or the temporal step size, whichever was larger, and was negligible for the results reported here. The white light was separated into two beams, signal and reference, to account for pulse-to-pulse spectral variations. Spectra were acquired using two spectrometers (Ocean Optics USB4000, 200−850 nm, 2 nm resolution). The polarization of the white light was set to the magic angle (54.7°) by rotating the polarization of the 800 nm input pulse.

The 266 nm pump pulse (∼2.5 μJ) and white light probe pulses (∼10 nJ) were focused at a relative angle of 14° into a 0.9-mm liquid flow cell (Harrick DCL-M25) using an 8″ focal length off axis paraboloid. The reference probe pulse was slightly displaced from the pumped volume. The sample was constantly exchanged so that each laser shot interacted with a fresh volume of the solution. The solutions were approximately 0.002 M *cis*-stilbene (Aldrich 96%) in *n*-hexane (Alfa Aesar spectro grade), used as received. Optimizations were performed probing 225 ps after the pump pulse, to allow decay of the transient absorption from the *trans*-stilbene[66] impurity and any vibrational cooling of the photoproducts.[54,56,66]

Experimental feedback values (fitness) for the *cis*- to *trans*-stilbene isomerization optimizations were evaluated by integrating over the 320−330 nm region of the transient absorption, where the difference in absorption between cis and trans was maximal. To account for shot-to-shot changes in the spectrum, a baseline value integrated over 350−360 nm was subtracted from the fitness value. This baseline wavelength range was chosen to be proximate to the cis to trans and DHP pump−probe features, while simultaneously being far enough from both peaks to be minimally affected by the absorptions.

For the DHP optimization experiments, a photodiode outfitted with low and high pass filters collected the integrated 400−500 nm DHP transient absorption signal to use as the fitness function. The spectral region between 400 and 500 nm contains only DHP absorption after the excited-state *trans*-stilbene decays, >200 ps. The pump was chopped at 500 Hz, and the differential diode signal was digitized using a boxcar (SR250) and an analog/digital converter (SR245).

Relative DHP to isomerization yield optimization experiments evaluated the experimental fitness values for the cyclization (400−500 nm) and isomerization (320−330 nm) by integrating over the appropriate regions of the transient absorption and subtracting out the integrated baseline (350−360 nm) value.

Shaped Pulse Measurement. Transient grating frequency-resolved optical gating (TG-FROG) was used to measure the shaped and unshaped 266 nm pulses. The 266 nm pulse was separated into three pulses and focused (box geometry) into a 1-mm sapphire plate while the time delay of one of the pulses was scanned. The four wave mixing signal was spectrally resolved in a home-built spectrometer (<0.4 nm resolution) at each delay time. This produced a background-free FROG signal equivalent to self-diffraction frequency-resolved optical gating (SD-FROG) with a reversal of the time delay axis but with higher sensitivity.[67] TG-FROG measurements were taken before and after optimization.

Learning Algorithms. We utilized several global and local optimization routines to search for the optimal pulse shape. The results were obtained with either an adaptive genetic algorithm modeled after previous reports,[68−70] the built-in downhill simplex algorithm of LabVIEW 8.0,[71] or a commercially available LabVIEW coding of the differential evolution algorithm.[72] The parameters of the search were usually five spectral phase coefficients of a sixth-order polynomial (the zero and first-order coefficients not affecting the pulse shape) along with five sine wave amplitudes and five sine wave frequencies, making 15 parameters altogether. Measurements were typically averaged to allow new parameter sets to be tested at ≥1 Hz. Downhill simplex runs would find solutions within 5 min before stagnating. Evolutionary methods would be run with a population of 15 individuals over 15 generations. Occasionally longer searches with up to 150 free parameters were employed, with results similar to those of the shorter optimizations. Start positions were randomized for all searches.

Results

The transient absorption spectrum of a 0.002 M *cis*-stilbene solution in *n*-hexane is shown in Figure 1a. The *z*-axis ($\Delta T/T$) of the contour plot describes the change in transmitted probe light normalized to the transmission without the 266 nm pump laser. There are three regions of interest. The first is between 320 and 330 nm and corresponds to the *cis*- to *trans*-stilbene isomerization. It reflects an increase in the concentration of the *trans*-stilbene isomer in the ground-state. The second region, between 400 and 500 nm, is associated with the cyclization of *cis*-stilbene to DHP and also represents an increase in ground-state concentration. The final region, between 575 and 600 nm, corresponds to an increase in concentration of excited-state *trans*-stilbene and is due to a *trans*-stilbene impurity in the initial *cis*-stilbene solution.

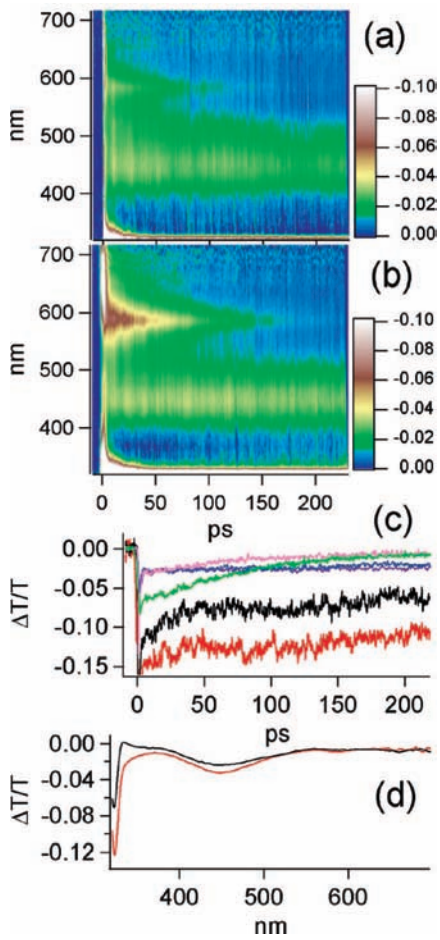

Figure 1. Transient absorption spectra obtained after minimization (a) and maximization (b) of *trans*-stilbene using a downhill simplex optimization routine. Pump/probe lineouts (c) for the cis to trans isomerization maximization (red) and minimization (black), DHP cyclization maximization (purple) and minimization (blue), and *trans*-stilbene excited-state maximization (green) and minimization (pink) are shown for the optimized pulses. Note that the optimization was performed only on the fitness of the isomerization product. Optimized phase (red) and no phase added (black) spectra (d) for the isomerization of *cis*-stilbene.

Line profiles of the pump−probe transients of the cis to trans, cis to DHP, and excited-state *trans*-stilbene are shown in Figure 1c. Spectra at 200 ps are shown in Figure 1d. At long times, the ground-state *trans*-stilbene and ground-state DHP signals remain constant and can be correlated with permanent photoproducts. Conversely, the excited-state *trans*-stilbene signal decays over time. Therefore, optimization of the *cis*- to *trans*-stilbene and cis to DHP was performed at 225 ps using two global routines (genetic algorithm and differential evolution) and one local routine (downhill simplex). Figure 1b shows the maximized transient absorption spectra obtained after using a downhill simplex routine to maximize the *cis*- to *trans*-stilbene signal.

Relative changes in the overall increased isomerization and cyclization fitnesses were found to be similar between the global and local optimizations (Table 1). The different optimization routines were carried out numerous times for the maximization and minimization of *trans*-stilbene and DHP. In all trials, we found that compressed pulses (Figure 2a) generated signal minimization while highly shaped pulses resulted in signal maximization (Figure 2b−g). Pulses that maximize yield are temporally stretched. Figure 2a−g shows the spectrograms obtained by TG-FROG measurement. No obvious common elements were found between the spectrograms visually or though Fourier analysis. Additional downhill simplex optimization experiments to control the relative yields of DHP to *trans*-stilbene were successful. The maximized DHP/*trans*-stilbene ratio of 0.272 ± 0.02 is indistinguishable from the compressed signal ratio (0.27 ± 0.01). The agreement of the maximization of the DHP-to-isomerization ratio occurs for compressed pulses, and the optimization process found that optimum. Conversely, a minimized signal of 0.23 ± 0.02 was obtained by decreasing pulse intensity, thereby optimizing the *trans*-stilbene signal.

Single parameter control schemes also influence the isomerization and cyclization reactions. Increasing the second-order spectral phase (linear chirp) of the electric field increased the *trans*-stilbene and DHP signal (Figure 3). Linear spectral phase is given in units of rad fs^2, but a more intuitive description is that 3.15×10^5 rad fs^2 corresponds to ~0.75 ps/nm. The spectral wings have intensity over more than 10 nm, but the FWHM is only 1.8 nm.

To test whether the yield was primarily affected by intensity decrease, the effect of pulse shaping was tested as a function of total pump energy. Figure 4 shows that the increased yield achieved by pulse shaping decreased at lower energies. This decrease occurs for optimal phase shapes determined either from a single high-energy optimization or for optimization at each pulse energy.

To test whether higher excited-states were affecting the yield, the intensity-dependent absorption was measured. The 266 nm pump transmission through the sample cell increased as linear chirp increased (Figure 5a) at high energy. The effect of chirp on the transmission was measured as the total pump energy was lowered (Figure 5b). Figure 5b illustrates that, at low energies, pulse length or intensity had little to no effect on transmission. Note that, while less light is absorbed by the sample, when the chirp is increased, the overall signal yield is increased.

The relative yields were measured as a function of pump pulse energy by recording the spectra at long times (225 ps) and normalizing to pump pulse energy, as shown in Figure 6a. The pump was fully compressed except as noted. Differences in the absolute yields for the isomerization and cyclization products as a function of energy are plotted in Figure 6b. At the lowest energy, we are at or asymptotically approaching the low intensity yield. Figure 6b shows that the high intensity yield of isomerization is 3.5 times smaller than the low intensity value of 33%; the high intensity isomerization yield is ~9%. Pulse shaping brings this back up to ~18%. As seen in Figure 6, isomerization and DHP production have different fitnesses as a function of energy.

Discussion

Each of the optimization routines found that compressed pulses minimized isomerization and cyclization efficiency while pulses of significant complexity maximized yield. Examination of the pulse shapes from the TG-FROG spectrograms shown in Figure 2 did not reveal any significant common features. Reproducible polynomial chirp profiles were only observed if an algorithm was repeatedly run from the same starting point. Fourier transforms of the temporal intensity did not reveal any common frequencies, as would be expected if the mechanism of yield enhancement contained any character of impulsively stimulated Raman. The only common feature observed between the optimal pulse shapes was a significant decrease in peak intensity from the compressed pulse.

Since pulse intensity can be controlled by a single parameter as opposed to the 15 parameter search of the optimization runs,

TABLE 1: Maximum/Unshaped Fitnesses Obtained from Optimization Routines and Single Parameter Control (Linear Chirp)

	downhill simplex	genetic algorithm	differential evolution	linear chirp
cis- to *trans*-stilbene isomerization	1.95 ± 0.11	1.83 ± 0.05	1.78 ± 0.1	1.46 ± 0.08
cis-stilbene to DHP cyclization	1.34 ± 0.1	1.47 ± 0.09	1.47 ± 0.01	1.45 ± 0.08

we examined the effect of scanning linear chirp. Linear chirp increased isomerization and cyclization efficiencies with success, as seen in Table 1. The asymmetry between positive and negative chirp of Figure 3 is not considered significant, the standard deviation of the values in Figure 3 is ~0.08, and examination of many data sets taken under similar conditions does not show reproducible asymmetry. The functional form of the fitness versus chirp shown in Figure 3 is strongly indicative of the underlying photophysical processes. Access to the first excited-state has no intensity dependence and would lead to a normalized yield of 1.0 independent of chirp. Introduction of a second excited-state populated proportional to the intensity squared leads to a curvature of the fitness versus chirp, as seen in Figure 3, but requires the isomerization and cyclization curves to have the same curvature as a function of intensity. This two excited-state model does not explain Figures 2 and 3 well. Introduction of a third excited-state populated proportional to the intensity cubed can produce fitnesses that have a maxima as a function of intensity and different shapes for the isomerization and cyclization curves. It seems that three excited-states are necessary to fully explain our data. The three-photon excited-state dominates only at the highest intensities, which then transitions to the two-photon excited-state at lower intensities and only the one-photon excited-state is available at low intensities. Each of these states can have different yields

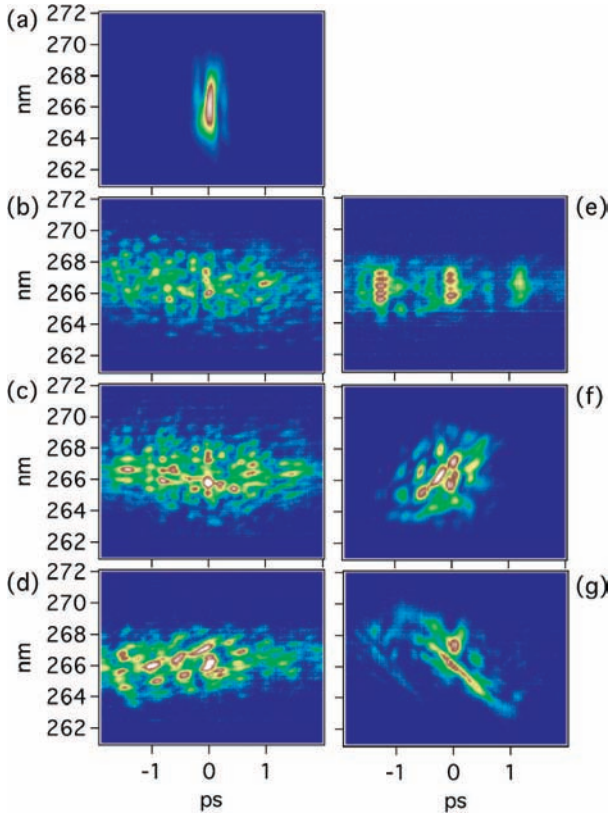

Figure 2. TG-FROG spectrograms. Minimized signal fitnesses come from optimally compressed pulses (a). Spectrograms of pulses that maximized the *cis*- to *trans*-stilbene isomerization obtained from downhill simplex (b), genetic algorithm (c), and differential evolution (d) optimization routines. Spectrograms of pulses that maximized cis to DHP cyclization obtained from downhill simplex (e), genetic algorithm (f), and differential evolution optimization routines. Note that intensity scales differ for the respective spectrograms.

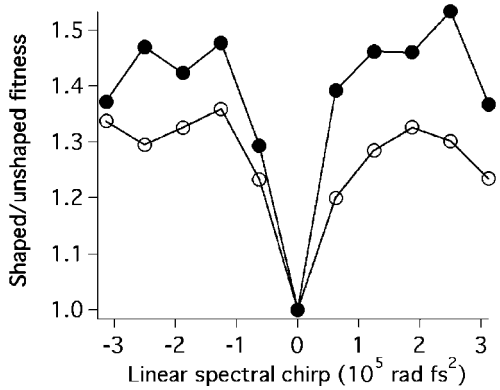

Figure 3. Ratio of maximized to unshaped fitness vs chirp. The *cis*- to *trans*-stilbene isomerization (●) and DHP cyclization (○) fitnesses increase with linear chirp. Pump energy is 2.8 μJ.

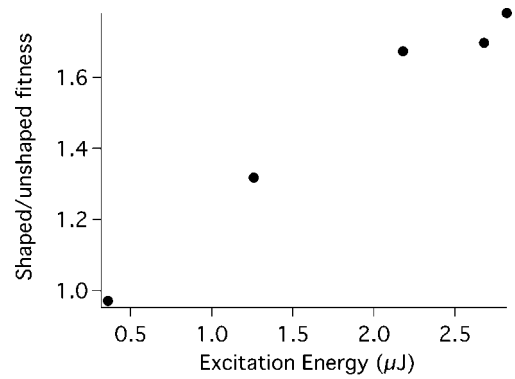

Figure 4. Maximized shaped/unshaped fitness is more effective at higher excitation energy.

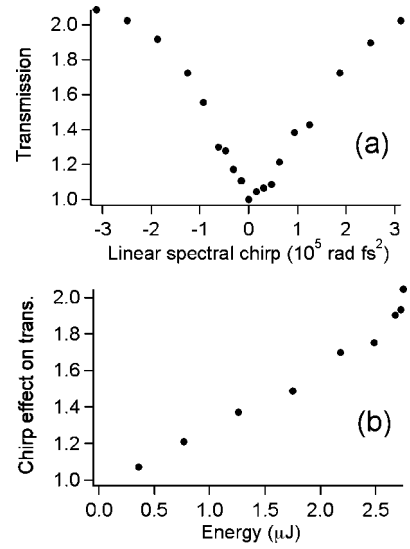

Figure 5. Increased relative transmission of the 266 nm pump pulse through the sample cell varies with respect to linear chirp at 2.7 μJ (a), but effect of spectral linear chirp at 3.1 × 10^5 rad fs^2 decreases with overall pump energy (b).

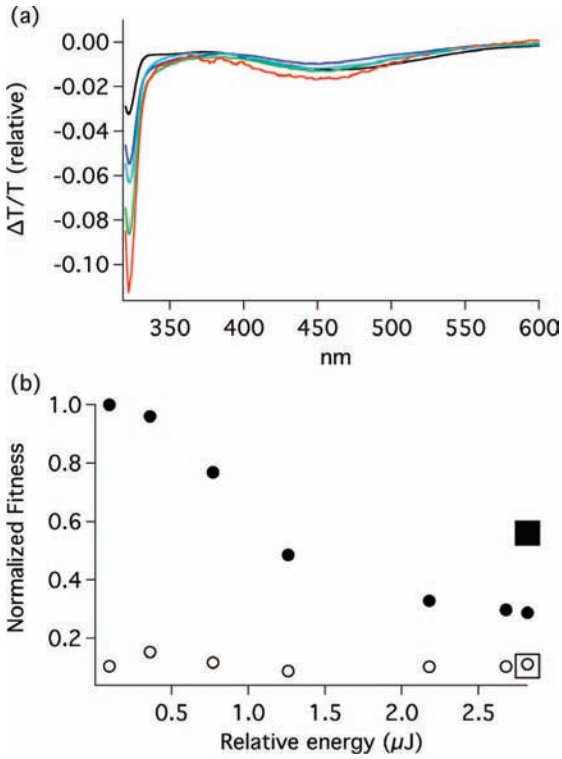

Figure 6. Pump/probe transient absorption spectra recorded at 225 ps, as a function of pump energy. Spectra are normalized to pump energy, to establish the intensity dependence of the isomerization and cyclization yields. Five spectra (a) of varying energy are shown: black (2.82 μJ), blue (1.26 μJ), green (0.77 μJ), red (0.1 μJ), and cyan (2.82 μJ, downhill simplex maximized pulse). (b) Relative isomerization (●) and cyclization (○) yields as a function of energy. Values obtained from a downhill simplex optimized pulse are shown as ■ (isomerization) and □ (cyclization).

for each of the photoproducts, and this is the mechanism by which yield control is achieved. Details of this model are provided in the Appendix, but the general conclusions are: (1) for yield to decrease with intensity, at least one higher-order state yield must be below the yield of the first excited-state, and (2) if there is an inflection point in the yield as a function of intensity, or if the curves of the product channels have different functional forms, at least three excited-states are needed. To produce an inflection point, the yield of the second and third excited-states relative to that of the first excited-state must change in sign. Further details are provided in the Appendix.

Another method of controlling intensity with a single parameter is to alter the total pulse energy. Figure 4 shows that the degree of yield enhancement upon pulse shaping depends strongly on the total energy of the pulse. The higher the energy, the more effective pulse shaping is in affecting the yield. This suggests that high intensity pulses produce excitations that have intrinsically lower yields for isomerization and cyclization product formation.

High intensity allows access to multiphoton transitions to higher excited electronic states. Evidence for this is the increased absorption of high intensity pulses, shown in Figure 5 as the transmission increased with increased pulse chirp (lowered intensity). Interestingly, the chirp required to maximize the yield and to increase the transmission is only about 1 ps. This correlates with the lifetime of the first excited-state of *cis*-stilbene in *n*-hexane, as measured by transient absorption at 650 nm, of 1.0 ps, a value in agreement with previous results.[59] It is likely that the resonant first excited-state is an intermediate in a sequential two-photon process, in accordance with the model of the Appendix.

Access to higher excited-states may open new channels to nonradiative decay. While this could occur directly from the higher excited-state (S_2, S_3, S_4, ...), a simpler interpretation would be relaxation through the first excited-state, but with far more excess energy than a single-photon excitation would allow. New relaxation channels may dominate on the first excited-state with the very large excess energies present following two-photon excitation. These experiments do not directly identify the relaxation channels but are only sensitive to their effect on the yield of isomerization and cyclization. The optimization experiments alone are measuring relative yields, but Figure 6 establishes that high intensities suppress the yield of isomerization by a factor of ~3.5, while the shaped pulse yield recovers a factor of 2 toward the low intensity yield. The fractional change in yield can be different for the isomerization and cyclization products upon pulse shaping, as shown in Figure 6b and explained in the Appendix. It is apparent from the incomplete recovery of yield ratio by pulse shaping that we have insufficient pulse shaping capabilities to fully achieve the low intensity regime at high pump energies.

While we have achieved significant yield changes, mostly due to intensity effects, even better control may be possible. The laser source used in these experiments produced 150 fs pulses at 266 nm. This bandwidth limits the ability to drive stimulated Raman processes to modes of frequencies below ~200 cm^{-1}. This excludes the excited-state double bond torsion[73] at 560 cm^{-1} that could potentially enhance the isomerization yield. Also, the peak pulse intensity could be increased to further enable higher excited-state participation. These limitations of the laser source may constrain the ability of coherent control beyond the intrinsic molecular limitations.

Conclusions

Shaped UV femtosecond pulses have been successfully employed to control the *cis*- to *trans*-stilbene isomerization as well as the *cis*-stilbene to DHP cyclization reactions. Global and local optimization routines yielded similar results in which the reactions were maximized for shaped pulses of significant complexity where the structure of the pulse shape was not crucial. The yields of both isomerization and cyclization were minimized for optimally compressed pulses. Linear chirp had a slightly smaller increase in yield than more complex pulse shapes, irrespective of the sign of the chirp. These and additional measurements implicated the presence of a multiphoton process with the *cis*-stilbene first excited-state as a probable intermediate. This multiphoton process is empirically found to diminish the isomerization and cyclization yield, while increasing the total energy absorbed. Avoiding the multiphoton effects is the mechanism by which the optimization processes achieved increase in yield. The article presents three main conclusions. (1) We document the experimental conditions in which multiphoton control is successful in controlling photoproduct branching ratios in stilbene. (2) The intensity dependence of the product yields can be used to map reactive channels of higher excited-states. (3) Under the experimental conditions employed (150 fs laser bandwidth), intensity control was the *only* mechanism available to the optimal control methods employed that could affect reaction yields.

Acknowledgment. We gratefully acknowledge the support of the U.S. Department of Energy through the LANL/LDRD

Program for this work. This work was performed, in part, at the Center for Integrated Nanotechnologies, a U.S. Department of Energy, Office of Basic Energy Sciences user facility. Los Alamos National Laboratory is operated by Los Alamos National Security, LLC, for the National Nuclear Security Administration of the U.S. Department of Energy under Contract DE-AC52-06NA25396. We also thank Dr. Mathias Roth for helpful advice in building the pulse shaper.

Appendix: Intensity Dependence Model

At low intensity, only the one-photon absorption is possible. The reaction yield, which here only depends upon intensity, is determined from previous low intensity measurements. As the intensity increases, a two-photon channel opens. Now, the reaction yield is a weighted average of the one- and two-photon channel reaction yields. This allows an intensity-dependent yield. As the intensity further increases, three-photon absorptions become possible and the total reaction yield becomes the weighted average of the yield of one-, two-, and three-photon absorption reaction yields. Three channels allow an inflection point in the intensity dependence of the reaction yield. The model below considers this in more detail.

The simplest model capable of explaining (1) the intensity dependence of the yields and (2) different intensity dependences for isomerization and cyclization yields is considered. Herein, we show that problem (1) is explained by introduction of a second excited-state, while problem (2) requires three excited-states. This simple model also shows how the functional form of the yields versus intensity provides information on the changes in yield for competing product channels present in each of the excited-states.

Consider the four-level system presented in Figure A1. S_0 is the ground-state, and S_1, S_n, and S_p are excited-states populated by sequential resonant multiphoton absorptions. The fraction of population in state j is f_j. We assume that $f_n = c_n I^2 - f_p$, $f_p = c_p I^3$, and $f_1 = 1 - (f_n + f_p)$; I is the laser intensity and c_j is the proportionality parameter for population of state j. The fractional yield for photoproduct P from state j is y_{jP}, and the sum over the three products from each state is unity, $\Sigma_P\, y_{jP} = 1$. The total yield of product P, Y_P, is then its sum over the yield from the individual states weighted by the fractional population of each state, $Y_P = \Sigma_j\, f_j y_{jP}$. Effects such as stimulated emission and Rabi oscillations are neglected to maintain the simplest possible model adequate to describe the intensity-dependent yields observed in the data.

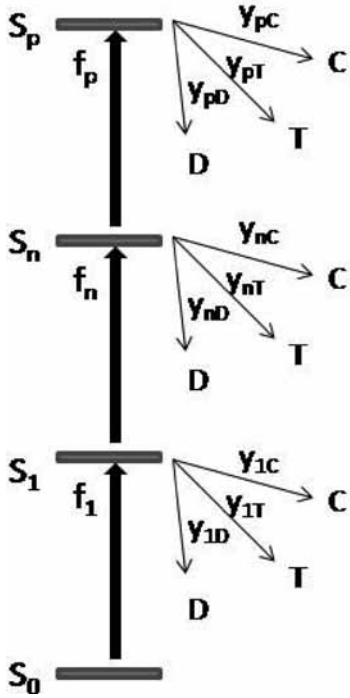

Figure A1. Four-level model. Each excited-state level, j, is populated to fraction f_j. Every level can have a different set of yields for final products, P, given by y_{jP}. The possible products considered are C = *cis*-stilbene, T = *trans*-stilbene, and D = dihydrophenanthrene. The yields from the first excited-state are known from the literature.[62]

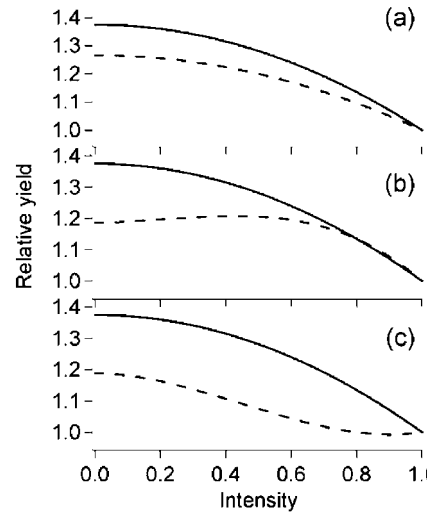

Figure A2. Calculations of intensity-dependent yields for the four-level model. The parameters are $y_{1T} = 0.33$, $y_{1D} = 0.19$. (a) $y_{nT} = 0.15$, $y_{nD} = 0.11$, $c_n = 0.5$, only two excited-states. (b) $y_{nT} = 0.18$, $y_{pT} = 0.18$, $y_{nD} = 0.28$, $y_{pD} = 0.0$, $c_n = 0.6$, $c_p = 0.3$. (c) $y_{nT} = 0.18$, $y_{pT} = 0.18$, $y_{nD} = 0.0$, $y_{pD} = 0.28$, $c_n = 0.6$, $c_p = 0.3$. Solid line corresponds to *trans*-stilbene final product and dashed line represents DHP final product.

Figure A2 illustrates the key predictions of the scheme presented in Figure A1. Figure A2a shows that two excited-states produce the same curvature of yield versus intensity for different products. This originates from the fact that the total yield for product P for two excited-state levels, ${}^{2\text{level}}Y_p = f_1 y_{1P} + f_n y_{nP} = (1 - f_n) y_{1P} + f_n y_{nP} = y_{1P} + f_n(y_{nP} - y_{1P})$. The intensity factor f_n is nonlinear, as seen in Figure A2a, but the only difference between the T product and the D product is the change in yield between the two excited-states; the term $(y_{nP} - y_{1P})$ is a constant and cannot introduce differences in curvature between the different products. The offset between the D and T products is due to the difference between $(y_{nD} - y_{1D})$ and $(y_{nT} - y_{1T})$. Adding a third excited-state level relieves this constraint, as differences between $(y_{nP} - y_{1P})$ and $(y_{pP} - y_{1P})$ can now cause inflection to occur as two-photon and three-photon processes compete. Figure A2b illustrates the effect of this competition, where the relative signs of $(y_{nP} - y_{1P})$ and $(y_{pP} - y_{1P})$ change and inflection occurs. Figure A2c shows the effect of changing the sign of both of these relative yield factors. Parameters of the model could not be reliably determined by a fit to the data of Figure 3. The qualitative features are easily interpreted in the following manner: (1) for yield to decrease with intensity, at least one higher-order state yield must be below the yield of the first excited-state, and (2) if there is an inflection point in the yield as a function of intensity, or if the curves of the product channels have different functional forms, at least three excited-states are needed. To produce an inflection point, the yield of the second and third excited-states relative to that of the first excited-state must change in sign. For the data of

Figure 3, a maximum in the yield versus intensity curve indicates that $y_{nP} > y_{1P}$ and $y_{pP} < y_{1P}$.

References and Notes

(1) Shapiro, M.; Hepburn, J. W.; Brumer, P. *Chem. Phys. Lett.* **1988**, *149*, 451.
(2) Brumer, P.; Shapiro, M. *Chem. Phys. Lett.* **1986**, *126*, 541.
(3) Tannor, D. J.; Rice, S. A. *Adv. Chem. Phys.* **1988**, *70*, 441.
(4) Palao, J. P.; Kosloff, R. *Phys. Rev. A* **2003**, *68*, 062308.
(5) Nakagami, K.; Ohtsuki, Y.; Fujimura, Y. *J. Chem. Phys.* **2002**, *117*, 6429.
(6) Levis, R. J.; Rabitz, H. A. *J. Phys. Chem. A* **2002**, *106*, 6427.
(7) Levis, R. J.; Menkir, G. M.; Rabitz, H. *Science* **2001**, *292*, 709.
(8) Kosloff, R.; Rice, S. A.; Gaspard, P.; Tersigni, S.; Tannor, D. J. *Chem. Phys.* **1989**, *139*, 201.
(9) Judson, R. S.; Rabitz, H. *Phys. Rev. Lett.* **1992**, *68*, 1500.
(10) Gong, J. B.; Rice, S. A. *Phys. Rev. A: At., Mol., Opt. Phys.* **2004**, *69*, 063410.
(11) Girardeau, M. D.; Schirmer, S. G.; Leahy, J. V.; Koch, R. M. *Phys. Rev. A: At., Mol., Opt. Phys.* **1998**, *58*, 2684.
(12) Geremia, J. M.; Zhu, W. S.; Rabitz, H. *J. Chem. Phys.* **2000**, *113*, 10841.
(13) Demiralp, M.; Rabitz, H. *Phys. Rev. A: At., Mol., Opt. Phys.* **1993**, *47*, 809.
(14) Brabec, T.; Krausz, F. *Rev. Mod. Phys.* **2000**, *72*, 545.
(15) Peirce, A. P.; Dahleh, M. A.; Rabitz, H. *Phys. Rev. A* **1988**, *37*, 4950.
(16) Bardeen, C. J.; Cao, J. S.; Brown, F. L. H.; Wilson, K. R. *Chem. Phys. Lett.* **1999**, *302*, 405.
(17) Nuernberger, P.; Vogt, G.; Brixner, T.; Gerber, G. *Phys. Chem. Chem. Phys.* **2007**, *9*, 2470.
(18) Lozovoy, V. V.; Dantus, M. *ChemPhysChem* **2005**, *6*, 1970.
(19) Dantus, M.; Lozovoy, V. V. *Chem. Rev.* **2004**, *104*, 1813.
(20) Brixner, T.; Gerber, G. *ChemPhysChem* **2003**, *4*, 418.
(21) Prokhorenko, V. I.; Nagy, A. M.; Waschuk, S. A.; Brown, L. S.; Birge, R. R.; Miller, R. J. D. *Science* **2006**, *313*, 1257.
(22) Otake, I.; Kano, S. S.; Wada, A. *J. Chem. Phys.* **2006**, *124*, 14501.
(23) Konradi, J.; Singh, A. K.; Scaria, A. V.; Materny, A. *J. Raman Spectrosc.* **2006**, *37*, 697.
(24) Florean, A. C.; Carroll, E. C.; Spears, K. G.; Sension, R. J.; Bucksbaum, P. H. *J. Phys. Chem. B* **2006**, *110*, 20023.
(25) Carroll, E. C.; Pearson, B. J.; Florean, A. C.; Bucksbaum, P. H.; Sension, R. J. *J. Chem. Phys.* **2006**, *124*, 114506.
(26) Buckup, T.; Lebold, T.; Weigel, A.; Wohlleben, W.; Motzkus, M. *J. Photochem. Photobiol., B* **2006**, *180*, 314.
(27) Vogt, G.; Krampert, G.; Niklaus, P.; Nuernberger, P.; Gerber, G. *Phys. Rev. Lett.* **2005**, *94*, 068305.
(28) Dudovich, N.; Oron, D.; Silberberg, Y. *J. Chem. Phys.* **2003**, *118*, 9208.
(29) Brixner, T.; Damrauer, N. H.; Kiefer, B.; Gerber, G. *J. Chem. Phys.* **2003**, *118*, 3692.
(30) Weinacht, T. C.; Bucksbaum, P. H. *J. Opt. B: Quantum Semiclassical Opt.* **2002**, *4*, R35.
(31) Dudovich, N.; Oron, D.; Silberberg, Y. *Nature* **2002**, *418*, 512.
(32) Damrauer, N. H.; Gerber, G. *ACS Symp. Ser.* **2002**, *821*, 190.
(33) Damrauer, N. H.; Dietl, C.; Krampert, G.; Lee, S. H.; Jung, K. H.; Gerber, G. *Eur. Phys. J. D* **2002**, *20*, 71.
(34) Bergt, M.; Brixner, T.; Dietl, C.; Kiefer, B.; Gerber, G. *J. Organomet. Chem.* **2002**, *661*, 199.
(35) Brixner, T.; Damrauer, N. H.; Niklaus, P.; Gerber, G. *Nature* **2001**, *414*, 57.
(36) Brixner, T.; Damrauer, N. H.; Gerber, G. *Adv. At., Mol., Opt. Phys.* **2001**, *46*, 1.
(37) Kunde, J.; Baumann, B.; Arlt, S.; Morier-Genoud, F.; Siegner, U.; Keller, U. *Appl. Phys. Lett.* **2000**, *77*, 924.
(38) Bartels, R.; Backus, S.; Zeek, E.; Misoguti, L.; Vdovin, G.; Christov, I. P.; Murnane, M. M.; Kapteyn, H. C. *Nature* **2000**, *406*, 164.
(39) Weinacht, T. C.; White, J. L.; Bucksbaum, P. H. *J. Phys. Chem. A* **1999**, *103*, 10166.
(40) Bergt, M.; Brixner, T.; Kiefer, B.; Strehle, M.; Gerber, G. *J. Phys. Chem. A* **1999**, *103*, 10381.
(41) Assion, A.; Baumert, T.; Bergt, M.; Brixner, T.; Kiefer, B.; Seyfried, V.; Strehle, M.; Gerber, G. *Science* **1998**, *282*, 919.
(42) Weinacht, T. C.; Ahn, J.; Bucksbaum, P. H. *Nature* **1999**, *397*, 233.
(43) Weiner, A. M. *Rev. Sci. Instrum.* **2000**, *71*, 1929.
(44) Tull, J. X.; Dugan, M. A.; Warren, W. S. *Adv. Magn. Opt. Res.* **1997**, *20*, 1.
(45) Wefers, M. M.; Nelson, K. A. *Opt. Lett.* **1995**, *20*, 1047.
(46) Weiner, A. M.; Leaird, D. E.; Patel, J. S.; Wullert, J. R. *Opt. Lett.* **1990**, *15*, 326.
(47) Weiner, A. M.; Leaird, D. E.; Patel, J. S.; Wullert, J. R. *IEEE J. Quantum Electron.* **1992**, *28*, 908.
(48) Roth, M.; Mehendale, M.; Bartelt, A.; Rabitz, H. *Appl. Phys. B* **2005**, *80*, 441.
(49) Schriever, C.; Lochbrunner, S.; Optiz, M.; Riedle, E. *Opt. Lett.* **2006**, *31*, 543.
(50) Pearson, B. J.; Weinacht, T. C. *Opt. Express* **2007**, *15*, 4385.
(51) Nuernberger, P.; Vogt, G.; Selle, R.; Fechner, S.; Brixner, T.; Gerber, G. *Appl. Phys. B* **2007**, *88*, 519.
(52) Waldeck, D. H. *Chem. Rev.* **1991**, *91*, 415.
(53) Waldeck, D. H. *J. Mol. Liq.* **1993**, *57*, 127.
(54) Repinec, S. T.; Sension, R. J.; Szarka, A. Z.; Hochstrasser, R. M. *J. Phys. Chem.* **1991**, *95*, 10380.
(55) Sension, R. J.; Repinec, S. T.; Hochstrasser, R. M. *J. Chem. Phys.* **1990**, *93*, 9185.
(56) Sension, R. J.; Repinec, S. T.; Szarka, A. Z.; Hochstrasser, R. M. *J. Chem. Phys.* **1993**, *98*, 6291.
(57) Sension, R. J.; Szarka, A. Z.; Hochstrasser, R. M. *J. Chem. Phys.* **1992**, *97*, 5239.
(58) Saltiel, J.; Waller, A. S.; Sears, D. F. *J. Photochem. Photobiol., A* **1992**, *65*, 29.
(59) Abrash, S.; Repinec, S.; Hochstrasser, R. M. *J. Chem. Phys.* **1990**, *93*, 1041.
(60) Baumert, T.; Frohnmeyer, T.; Kiefer, B.; Niklaus, P.; Strehle, M.; Gerber, G.; Zewail, A. H. *Appl. Phys. B* **2001**, *72*, 105.
(61) Quenneville, J.; Martinez, T. J. *J. Phys. Chem. A* **2003**, *107*, 829.
(62) Rodier, J. M.; Myers, A. B. *J. Am. Chem. Soc.* **1993**, *115*, 10791.
(63) Bearpark, M. J.; Bernardi, F.; Clifford, S.; Olivucci, M.; Robb, M. A.; Vreven, T. *J. Phys. Chem. A* **1997**, *101*, 3841.
(64) Yamaguchi, S.; Hamaguchi, H. O. *Appl. Spectrosc.* **1995**, *49*, 1513.
(65) Roth, M.; Feurer, T.; Sauerbrey, R. *Z. Phys. Chem. (Muenchen, Ger.)* **2001**, *215*, 1557.
(66) Kovalenko, S. A.; Schanz, R.; Hennig, H.; Ernsting, N. P. *J. Chem. Phys.* **2001**, *115*, 3256.
(67) Trebino, R.; DeLong, K. W.; Fittinghoff, D. N.; Sweetser, J. N.; Krumbugel, M. A.; Richman, B. A.; Kane, D. J. *Rev. Sci. Instrum.* **1997**, *68*, 3277.
(68) Goldberg, D. E. *Genetic algorithms in search, optimization, and machine learning*; Addison-Wesley: Reading, MA, 1989.
(69) Davis, L. *Handbook of genetic algorithms*; Van Nostrand Reinhold: New York, 1991.
(70) Pearson, B. J.; White, J. L.; Weinacht, T. C.; Bucksbaum, P. H. *Phys. Rev. A: At., Mol., Opt. Phys.* **2001**, *63*, 063412.
(71) LabVIEW, 8.0 ed.; National Instruments: Austin, TX, 2007.
(72) Price, K. V.; Storn, R. M.; Lampinen, J. A. *Differential evolution*; Springer Verlag: New York, 2005.
(73) Myers, A. B.; Mathies, R. A. *J. Chem. Phys.* **1984**, *81*, 1552.

JP801758V